

Alfvén Instabilities in DIII-D: Fluctuation Profiles, Thermal-Ion Excitation, and Fast-Ion Transport

W.W. Heidbrink 1), G.J. Kramer 2), R. Nazikian 2), M.A. Van Zeeland 3), M.E. Austin 4),
H.L. Berk 4), K.H. Burrell 5), N.N. Gorelenkov 2), Y. Luo 1), G.R. McKee 6),
T.L. Rhodes 7), G. Wang 7), and the DIII-D Team

- 1) University of California, Irvine, California, USA
- 2) Princeton Plasma Physics Laboratory, Princeton, New Jersey, USA
- 3) Oak Ridge Institute for Science Education, Oak Ridge, Tennessee, USA
- 4) University of Texas, Austin, Texas, USA
- 5) General Atomics, San Diego, California, USA
- 6) University of Wisconsin, Madison, Wisconsin, USA
- 7) University of California, Los Angeles, California, USA

e-mail contact of main author: Bill.Heidbrink@uci.edu

Abstract. New fluctuation and fast-ion diagnostics provide a wealth of data about fast-ion instabilities during neutral beam injection into DIII-D. Toroidicity-induced Alfvén eigenmodes (TAE), reversed-shear induced Alfvén eigenmodes (RSAE), and compressional Alfvén eigenmodes are observed. Owing to differing spatial sensitivities, the measured spectra differ greatly for different diagnostics. In plasmas with reversed shear, the radial profiles of electron temperature and electron density fluctuations agree well with the predictions of linear magnetohydrodynamics for both TAEs and RSAEs. The Doppler shift due to plasma rotation often has a strong effect on the observed RSAE frequency. Estimates based on the Doppler shift indicate that, in plasmas with a large gradient in ion temperature, the toroidal mode number approaches 40. The measured poloidal wavenumber is also large ($\lesssim 0.8 \text{ cm}^{-1}$). These measurements and supporting calculations suggest that thermal ions drive RSAEs in these high temperature plasmas. The Alfvén eigenmodes degrade the fast-ion confinement and the degradation increases with increasing beam power. The evolution of the q profile is also altered by the fast-ion transport.

1. Introduction

Alpha particles may drive Alfvén eigenmodes unstable in ITER and other burning plasma experiments. If they do, the most important practical issue is the resultant fast-ion transport. Will benign local flattening of the alpha pressure profile occur, or will the alphas escape from the plasma and damage the vessel wall? Remarkably, in the two most detailed quantitative investigations of this important issue, the calculated transport by toroidicity-induced Alfvén eigenmodes (TAE) is much smaller than the measured losses [1,2]. To resolve this discrepancy and benchmark theoretical predictions for ITER, detailed measurements of internal fluctuations and of fast-ion profiles are essential.

Improved fluctuation and fast-ion diagnostics on DIII-D can now address this important issue. Several diagnostic systems have improved sensitivity and bandwidth for the detection of Alfvén modes. CO₂ interferometers measure line-integrated density fluctuations along four spatial chords [3]. Far-infrared 300 GHz low- k scattering also measures the line integral of the density fluctuations. Microwave quadrature reflectometers provide local density fluctuation measurements [4], as does an upgraded, high throughput, beam emission spectroscopy (BES) diagnostic [5]. The upgraded electron cyclotron emission (ECE) diagnostic provides local electron temperature fluctuation measurements at 40 radial positions [6].

A new fast-ion diagnostic uses the charge-exchange recombination light from fast deuterium ions that neutralize in a heating beam [7]. This fast-ion D_α (FIDA) diagnostic currently consists of one instrument that measures the full spectrum at two radial locations [8] and another instrument that measures partial spectra at seven radial positions. Accurate background subtraction through beam modulation and other techniques is required to extract valid fast-ion signals from the measured spectra [9]. The resolution achieved with the FIDA diagnostic is ~ 10 keV in energy, ~ 5 cm in space, and ~ 1 ms in time [9].

In this paper, these diagnostics are applied to TAE, reversed-shear Alfvén eigenmode (RSAE), and compressional Alfvén eigenmode (CAE) instabilities that are generated during injection of ~ 80 keV deuterium neutral beams into DIII-D. Recent publications and results are summarized within the context of a particular set of reversed-shear discharges from the 2005 experimental campaign.

2. Fluctuation Data

In the principal discharge under investigation, beam injection commences during the current ramp to form an off-axis minimum in the safety factor profile q ; this q_{\min} steadily decreases as the current diffuses [Fig. 1(a)]. The plasma density is kept at a relatively low value of $\simeq 2 \times 10^{19} \text{ m}^{-3}$ [Fig. 1(b)], so the fast-ion pressure is a significant fraction of the total plasma pressure [Fig. 1(d)]. The discharge is initially in an inner wall limiter configuration (Fig. 2) then switches to a double-null divertor configuration at 400 ms. The electron temperature increases steadily throughout the current ramp [Fig. 1(b)]; the ion temperature is $\sim 20\%$ higher than T_e . Near-tangential ($R_{\tan} = 1.15$ m) neutral beam injection in the co-current direction is employed, so the toroidal rotation f_{rot} increases early in the discharge and maintains a steady value of ~ 9 kHz subsequently [Fig. 1(c)]. Throughout the period of interest, the velocity of the full-energy neutrals v_{beam} exceeds $0.4 v_A$ (v_A is the Alfvén speed), so excitation of TAEs by circulating fast ions at the $v_A/3$ sideband resonance is expected [Fig. 1(c)]. The neutron rate steadily increases throughout the current ramp, as does the local fast-ion density inferred from the FIDA diagnostic [Fig. 1(e)].

The spatial location of several important diagnostics is illustrated in Fig. 2. At the selected toroidal field of 2.0 T, ECE radiometer channels span the entire outer half of the plasma.

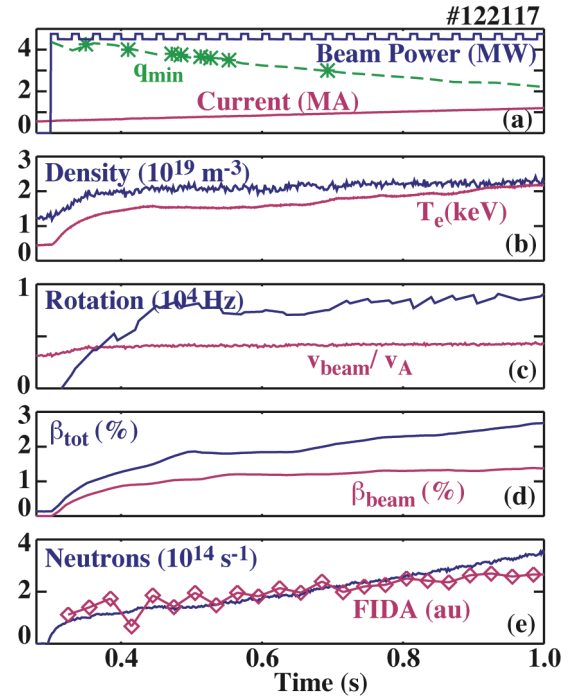


FIG. 1. Time evolution of (a) neutral beam power, plasma current, q_{\min} from equilibrium reconstruction (dashed curve), and q_{\min} inferred from the RSAE cascades (individual points), (b) line-average electron density \bar{n}_e and central electron temperature, (c) central toroidal rotation frequency from charge-exchange recombination spectroscopy of carbon impurities and ratio of the speed of injected 81 keV deuterium ions to the Alfvén speed evaluated using the vacuum magnetic field (2.0 T) and \bar{n}_e , (d) central toroidal β and central beam-ion β from TRANSP assuming neoclassical fast-ion behavior, and (e) measured neutron rate and FIDA “density” at 1.94 m.

An array of 16 high-resolution BES channels measure the fluctuations from a relatively small region of the plasma that is located near the q_{\min} surface, which occurs at a normalized minor radius of $\rho_{q\min} = 0.45$ in these plasmas. Vertical and radial CO₂ interferometer chords also traverse this region. FIDA channels span from the outer edge to the magnetic axis; the data in this paper are from the region near $\rho_{q\min}$. Mirnov coils with 250 kHz bandwidth measure edge fluctuations in the vertical magnetic field; in addition, single-turn toroidal loops with a plasma-facing graphite front surface [10] measure fluctuations up to 50 MHz.

The fluctuation diagnostics observe a large number of instabilities in the Alfvén frequency band in these plasmas (Fig. 3). Some modes have relatively constant frequencies, while others have frequencies that approximately double on a 30 ms timescale. The modes with nearly constant frequencies are TAEs; since the Alfvén speed and rotation frequency are approximately stationary (Fig. 1), the expected TAE frequency in the laboratory frame is $f_{\text{lab}} \approx v_A/(4\pi q R) + n f_{\text{rot}} \approx 70 + 20 = 90$ kHz and evolves gradually in time. (Here R is the major radius and n is the toroidal mode number. [The prominent 85 kHz mode in Fig. 3(a) has $n = 3$.] The modes that sweep upward in frequency are RSAEs. Theoretically, the frequency of a RSAE in the plasma frame is

$$f_{\text{RSAE}} = f_{\min} + \frac{(m - nq_{\min})v_A}{2\pi q_{\min} R}, \quad (1)$$

where f_{\min} is an initial frequency that depends on plasma pressure [11]. Since the poloidal mode number m initially equals nq_{\min} and q_{\min} steadily decreases, the RSAE frequency rapidly increases as the quantity $m - nq_{\min}$ increases.

The differences in the spectra measured by the various diagnostics are striking. The ECE signal from a region well outside $\rho_{q\min}$ essentially only detects TAEs [Fig. 3(a)]. In contrast, the ECE signal near $\rho_{q\min}$ is dominated by RSAE activity [Fig. 3(b)]. The Mirnov coil sees primarily TAEs [Fig. 3(c)]. Cross-power spectra from vertical and radial CO₂ interferometer channels clearly detect both TAEs and RSAEs [Fig. 3(d)]. The BES spectra from $\rho_{q\min}$ are dominated by RSAEs [Fig. 3(e)].

Differences such as these are commonplace and are readily explained by the differing spatial sensitivities of the diagnostics, together with the different spatial eigenfunctions of TAEs and RSAEs. RSAEs are radially localized instabilities with a single dominant poloidal harmonic. In contrast, TAEs are globally extended modes comprised of several poloidal harmonics. RSAEs are rarely visible on magnetics signals because the localized spatial eigenfunction has

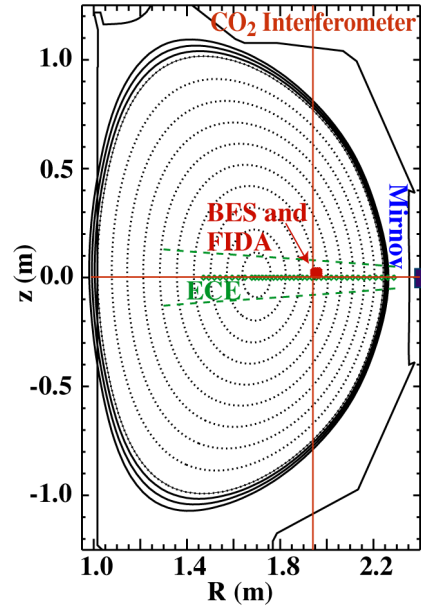


FIG. 2. Spatial location of the fluctuation and fast-ion measurements for the data shown in subsequent figures. The dotted curves show the equilibrium at 410 ms in discharge #122117. The diamonds indicate the position of the ECE channels; the dashed lines represent the Gaussian beam waist of the ECE antenna pattern.

a negligibly small amplitude at the vessel wall. A necessary condition to detect RSAEs is a sensitivity to fluctuations near $\rho_{q\min}$. This alone is not sufficient, however. For a line-integrated measurement, cancellations caused by the poloidal mode structure can obscure the presence of some modes [3,12]. In a typical DIII-D discharge such as the one discussed here, the TAEs are clearest on the vertical interferometer chords, while the RSAEs are most apparent on the radial chord.

Detailed measurements of the radial structure are obtained with the ECE radiometer (Fig. 4) [12]. The RSAE eigenfunction extends radially over ~ 0.15 in ρ , while the TAE eigenfunction spans about half of the minor radius. To within the accuracy of the equilibrium reconstruction, the maximum amplitude of the RSAE eigenfunction occurs at the minimum of the q profile. The peak measured temperature perturbation of $\delta T_e/T_e \approx 0.5\%$ is of similar magnitude for both TAEs and RSAEs.

The measured RSAE and TAE mode structures are in excellent agreement with the predictions of linear ideal MHD theory [13]. Figure 5(a) compares the prediction of the NOVA [14] MHD code with the ECE measurements for a $n = 3$ RSAE. Within experimental errors, the shape of the modeled eigenfunction is in excellent agreement with experiment. To obtain this comparison, the eigenfunction calculated by NOVA is processed by a synthetic diagnostic that includes the spatial sensitivity of the actual ECE diagnostic (Fig. 1). Since NOVA is a linear MHD code, the amplitude of the theoretical eigenfunction has been adjusted to match the data. Once this amplitude is selected, however, the magnitude of the predicted density fluctuations is fixed. Figure 5(b) shows that the predicted density fluctuations are in excellent agreement in both magnitude and shape with independent measurements of $\delta n_e/n_e$ by the BES and reflectometer diagnostics. Similar agreement between experiment and linear MHD theory is observed for a $n = 3$ TAE

Further confirmation of the validity of the ideal MHD model is obtained when the RSAE frequency sweeps past the TAE frequency. At these times, the RSAEs and TAEs couple and mix in structure, in striking agreement with NOVA predictions of the mode structure [15]. (The phenomena are similar to coupling between core TAEs and global TAEs observed in JT-60U [16].)

The toroidal mode numbers of the RSAEs can be quite large. In the discharges shown here (Fig. 1), the largest inferred toroidal mode number is $n \sim 20$. For these large values of n , the

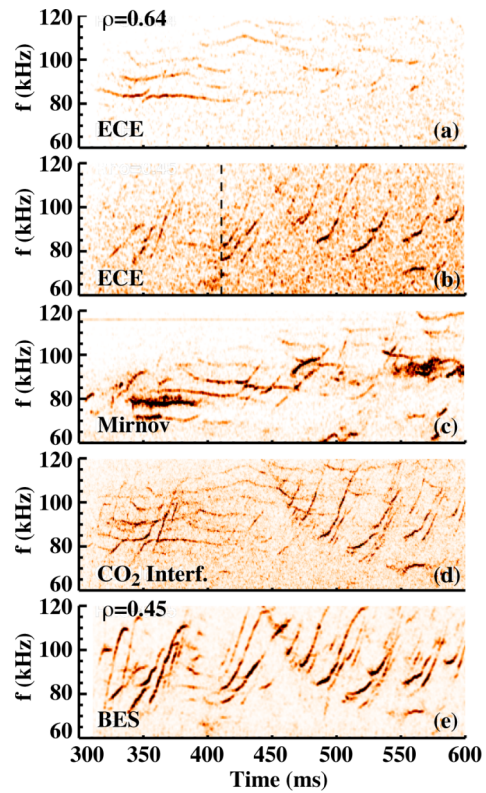


Fig. 3. Spectra from several fluctuation diagnostics. (a) Power spectrum of ECE radiometer data for the channel that is at a radial position of $\rho = 0.64$ at $t = 410$ ms. (ρ = normalized square root of the toroidal flux). (b) Power spectrum of ECE radiometer data for the $\rho = 0.45$ channel. (c) Mirnov coil power spectrum. (d) Interferometer cross-power spectrum of a vertical chord and a radial chord. (e) BES cross-power spectrum of adjacent channels that are near $\rho = 0.45$.

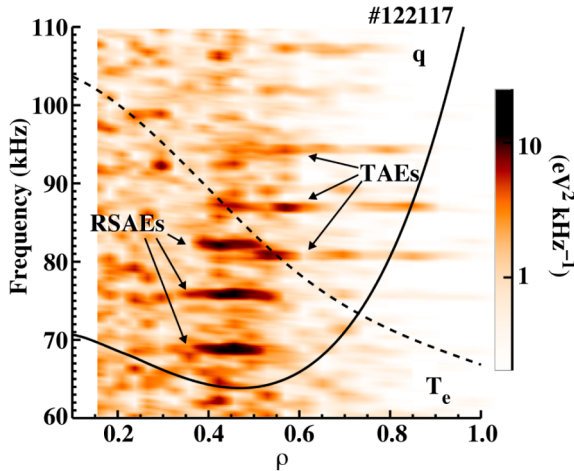


FIG. 4. Radial profile of ECE power spectra. The frequencies of the modes marked RSAEs sweep in time while the modes marked TAEs have relatively steady frequencies. The q and T_e profiles are shown in arbitrary units; $q_{\min} \approx 4.0$ and $T_e(0) = 1.5$ keV.

Doppler shift nf_{rot} can dominate the observed frequency [17]. In DIII-D discharges where the current is reversed from its usual direction, the direction of mode propagation in the plasma frame is opposite to the sign of the Doppler shift. As a result, the RSAE frequency sweeps downward in time rather than the usual upward frequency sweep. The observed frequency evolution is still readily explained by Eq. (1). As expected, in plasmas with co-injection, the usual upward frequency sweeping is observed.

The largest values of n are observed in plasmas with internal transport barriers and $T_i > 10$ keV. The toroidal mode number inferred from the frequency evolution reaches $n = 40$ in these plasmas [18]. These short spatial scales are corroborated by BES measurements of the poloidal wavenumber, which find $k_\theta \lesssim 0.8$ cm $^{-1}$. The n and k_θ measurements indicate a mode structure that varies on the scale of the thermal ion Larmor radius. Stability calculations suggest that thermal ions are largely responsible for destabilization of these high- n modes.

In addition to Alfvén instabilities in the 100 kHz band, instabilities are often observed with sub-cyclotron frequencies of a few MHz [19,20]. The strong resemblance between these instabilities and modes observed in NSTX suggests that they are compressional Alfvén eigenmodes. These modes are probably driven by a bump in the velocity distribution. The modes are most readily observed at low toroidal magnetic field ($B_T \lesssim 1.2$) but are sometimes observed at 2.0 T as well. For example, in the discharge illustrated in Fig. 1, intermittent modes with frequencies of about 5 MHz occur.

3. Fast-Ion Data

Data from four independent diagnostics show that the RSAE and TAE instabilities shown in Fig. 3 have a strong effect on fast-ion confinement.

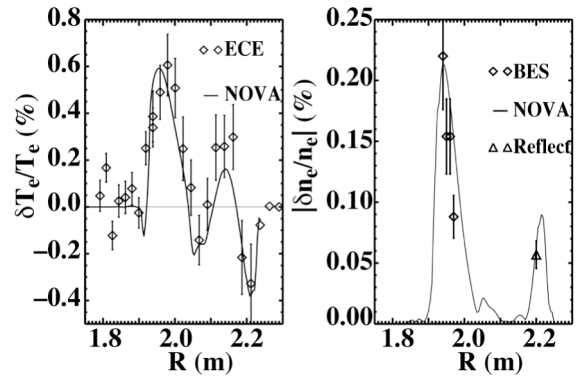


FIG. 5. (a) Comparison of the normalized temperature fluctuation measured by ECE (symbols) with the normalized temperature fluctuation predicted by NOVA (solid) for the 76 kHz $n = 3$ RSAE. The amplitude of the NOVA eigenfunction has been scaled to fit the data. (b) Comparison of the normalized density fluctuation measured by BES (diamonds) and the quadrature reflectometer (triangle) with the NOVA prediction for the same mode. There are no free parameters in this comparison (#122117).

Measurements of the volume-averaged neutron rate from five sequential discharges with increasing amounts of beam power are shown in Fig. 6. The TRANSP code [21] calculates the fast-ion distribution function assuming classical deceleration and confinement. As shown in Fig. 6(b), the ratio of the measured volume-average neutron rate to the TRANSP predictions is $\lesssim 0.5$ during the intense Alfvén activity. Beam-plasma reactions dominate the neutron rate in these plasmas, so a reduction in the neutron rate below the TRANSP prediction indicates that fast ions are redistributed or lost from the plasma. Given the complexity of the Alfvén spectra, it is difficult to quantify the overall amplitude of Alfvén activity but the bandpass-filtered Mirnov coil signal shown in Fig. 6(a) is a reasonable measure of the global modes that are expected to dominate fast-ion transport. As the beam power increases, the amplitude of Alfvén activity tends to increase. Comparison with the neutron signals shows that the neutron deficit grows larger with increasing beam power as well; in addition, the time evolution of the deficit within a shot is also correlated with the amplitude of Alfvén activity. This correlation strongly suggests that the Alfvén modes are responsible for the degraded fast-ion confinement.

FIDA data support this conclusion. The FIDA signals are proportional to the product of the fast-ion density n_f and the injected neutral density n_0 . For the data shown here, the FIDA spectra are first averaged over 10 ms, then the backgrounds (obtained by beam modulation) are subtracted from the spectra. Next, the spectra are integrated over the wavelengths that correspond to perpendicular energies between 30–80 keV. The FIDA fast-ion “density” shown in Fig. 1(e) is this signal divided by the injected neutral density. The dominant errors in this FIDA density are associated with systematic errors in the background subtraction (typically $\sim 15\%$). Figure 6(c) compares this fast-ion density for the channel near $\rho_{q\min}$ with the beam density predicted by TRANSP. The result is nearly identical to the neutron comparison in Fig. 6(b): the deficit increases with increasing beam power and, within a discharge, the time evolution correlates with the evolution of the Alfvén amplitude. FIDA profile measurements at selected time slices show that the fast-ion density profile is nearly flat inside $\rho = 0.6$ during the strong Alfvén activity shown in Fig. 3.

Further evidence of fast-ion redistribution is obtained from equilibrium reconstructions using the EFIT [22] code. The input data for these reconstructions are external magnetics, internal vertical field measurements from the motional Stark effect (MSE) diagnostic, the radial position of flux surfaces (particularly the magnetic axis) from ECE measurements (assuming T_e is a flux function), and the pressure profile from thermal ion and electron diagnostics in

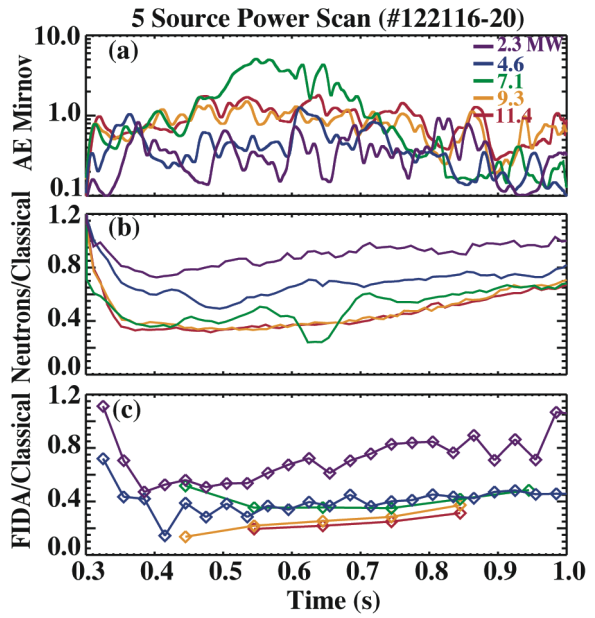


FIG. 6. (a) Amplitude of magnetic fluctuations between 60–120 kHz, (b) ratio of the measured neutron rate to the rate predicted by TRANSP assuming neoclassical fast-ion confinement, and (c) ratio of the FIDA signal at $R = 1.94$ m to the fast-ion density predicted by TRANSP at the same minor radius for five similar discharges with injected beam powers of 2.3, 4.6, 7.1, 9.3, and 11.4 MW, respectively.

the outer 40% of the plasma. The pressure profile is obtained from the equilibrium reconstruction. Then, after subtraction of the measured thermal pressure, the fast-ion pressure is inferred. Like the FIDA profile, this fast-ion pressure profile is nearly flat at 365 ms and the pressure on axis is only 40% of the TRANSP prediction.

The fourth sign of fast-ion redistribution is anomalous evolution of the current profile. The TRANSP code can predict the evolution from the poloidal current diffusion equation using the neoclassical resistivity and bootstrap current profiles inferred from input data. The plasma loop voltage is adjusted to match the measured current. Neutral beam driven currents can be included or excluded. In either case, TRANSP predicts that the safety factor decreases much faster than observed experimentally; $\rho_{q\min}$ also contracts more slowly in the experiment than in the calculation. Apparently, in the experiment, the Alfvén eigenmodes transport neutral beam ions from the magnetic axis to $\rho \approx 0.5$, creating a current profile that is much broader than otherwise expected. This phenomenon has been observed and analyzed previously [23] and seems to occur in the majority of DIII-D discharges with early beam injection. In the discharge considered here, the RSAEs provide strong additional evidence that the current evolution is anomalous. First, at 785 ms, the value of q_{\min} inferred from the RSAE activity and $\rho_{q\min}$ inferred from the ECE profile data are larger than predicted by TRANSP. Second, with neoclassical fast-ion confinement and ordinary neutral-beam current drive, the TRANSP code predicts that the q profile becomes monotonic at 950 ms but upward chirping RSAEs are clearly visible on the FIR scattering diagnostic through 1450 ms.

4. Implications for ITER

Theoretical models that have been benchmarked by experiment are required for reliable predictions of Alfvén activity and alpha-particle transport in ITER. The linear stability, mode structure, nonlinear dynamics, and consequent fast-ion transport must all be understood.

On linear stability, the recent observations make two important contributions. First, the observation of CAEs in DIII-D suggests that these modes may be driven unstable by alpha particles in ITER. Second, the small spatial scale of the highest n modes suggests an interaction of Alfvén waves with thermal ions, as was predicted in earlier theories [24].

On mode structure, previous DIII-D comparisons with data from a less complete set of fluctuation diagnostics found poor agreement with the linear MHD model [1,25]. In contrast, the agreement of linear MHD with the present data is excellent. The previous work was in a strongly-driven, low toroidal-field regime, so it is possible that the “TAEs” in the previous work were actually energetic particle modes. Unstable modes in ITER are unlikely to be strongly driven, so the present results support the use of the MHD eigenfunction in ITER predictions.

On nonlinear dynamics, if Alfvén instabilities are unstable in ITER, a large number of moderate n modes are expected to be unstable simultaneously. The observation of many unstable moderate n modes in DIII-D suggests that it may be possible to study the nonlinear physics of a “sea” of interacting Alfvén eigenmodes in DIII-D.

On consequent transport, calculations are underway to compute fast-ion transport in the Alfvén waves computed by NOVA. Once these calculations are complete, the modified distribution function will be compared with the FIDA and neutron data. The modified distribution function will also be used to calculate a modified neutral-beam current profile for

comparison with the observed q profile evolution and plasma equilibrium. If these comparisons show quantitative agreement, credible predictions of alpha transport in ITER will follow.

This work was supported by the U.S. Department of Energy under SC-G903402, DE-AC02-76CH03073, DE-AC05-76OR00033, DE-FG03-97ER54415, DE-FC02-04ER54698, DE-FG02-89ER53297, and DE-FG03-01ER54615.

References

- [1] CAROLIPIO, E. M., HEIDBRINK, W. W., CHENG, C. Z., et al., Phys. Plasma **8** (2001) 3391.
- [2] TODO, Y., BERK, H. L., BREIZMAN, B. N., et al., Phys. Plasma **10** (2003) 2888.
- [3] VAN ZEELAND, M. A., KRAMER, G. J., NAZIKIAN, R., et al., Plasma Phys. Controlled Fusion **47** (2005) L31.
- [4] WANG, G., PEEBLES, W. A., RHODES, T. L., et al., Nucl. Fusion **46** (2006) S708.
- [5] GUPTA, D. K., FONCK, R. J., MCKEE, G. R., SCHLOSSBERG, D. J., and SHAFER, M. W., Rev. Sci. Instrum. **75** (2004) 3493.
- [6] AUSTIN, M. E. and LOHR, J., Rev. Sci. Instrum. **74** (2003) 1457.
- [7] HEIDBRINK, W. W., BURRELL, K. H., LUO, Y., PABLANT, N. A., and RUSKOV, E., Plasma Phys. Controlled Fusion **46** (2004) 1855.
- [8] LUO, Y., BURRELL, K. H., and HEIDBRINK, W. W., Rev. Sci. Instrum. **75** (2004) 3468.
- [9] LUO, Y., HEIDBRINK, W. W., BURRELL, K. H., GOHIL, P., and KAPLAN, D., Rev. Sci. Instrum. **77** (2006) submitted.
- [10] WATSON, G. W. and HEIDBRINK, W. W., Rev. Sci. Instrum. **74** (2003) 1605.
- [11] BREIZMAN, B. N., PEKKER, M. S., SHARAPOV, S. E., et al., Phys. Plasma **12** (2005) 112506.
- [12] VAN ZEELAND, M. A., AUSTIN, M. E., CARLSTROM, T.N., et al., Nucl. Fusion **46** (2006) S880.
- [13] VAN ZEELAND, M. A., KRAMER, G. J., AUSTIN, M. E., et al., Phys. Rev. Lett. **97** (2006) 135001.
- [14] CHENG, C. Z., Phys. Reports **1** (1992) 211.
- [15] VAN ZEELAND, M. A. et al., Phys. Plasma **14** (2007) to be submitted.
- [16] KRAMER, G. J., CHENG, C. Z., FU, G. Y., et al., Phys. Rev. Lett. **83** (1999) 2961.
- [17] KRAMER, G. J., NAZIKIAN, R., ALPER, B., et al., Phys. Plasma **13** (2006) 056104.
- [18] NAZIKIAN, R., BERK, H. L., BUDNY, R. V., et al., Phys. Rev. Lett. **96** (2006) 105006.
- [19] HEIDBRINK, W. W., FREDRICKSON, E. D., GORELENKOV, N. N., RHODES, T., and VAN ZEELAND, M. A., Nucl. Fusion **46** (2006) 324.
- [20] WANG, G., PEEBLES, W. A., RHODES, T. L., et al., Nucl. Fusion **46**, (2006) S708.
- [21] BUDNY, R. V., Nucl. Fusion **34** (1994) 1247.
- [22] LAO, L. L., ST JOHN, H., STAMBAUGH, R. D., KELLMAN, A. G., and PFEIFFER, W., Nucl. Fusion **25** (1985) 1611.
- [23] WONG, K. L., BUDNY, R., NAZIKIAN, R., et al., Phys. Rev. Lett. **93** (2004) 085002; WONG, K. L., HEIDBRINK, W. W., RUSKOV, R., et al., Nucl. Fusion **45** (2005) 30.
- [24] ZONCA, F., CHEN, L., and SANTORO, R. A., Plasma Phys. Controlled Fusion **38** (1996) 2011.
- [25] HEIDBRINK, W. W., JAUN, A., and HOLTIES, H. A., Nucl. Fusion **37** (1997) 1411.